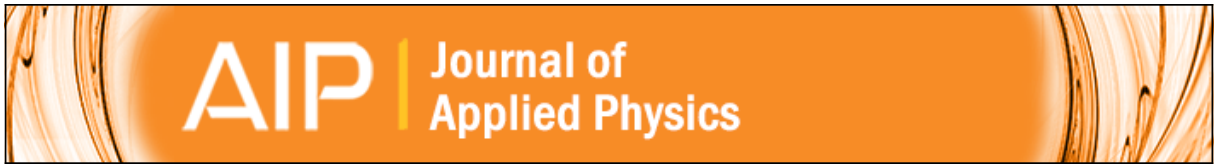

Multiple scattering x-ray photoelectron diffraction study of the SrTiO 3 (100) surface

A. Pancotti, N. Barrett, L. F. Zagonel, and G. M. Vanacore

Citation: Journal of Applied Physics **106**, 034104 (2009); doi: 10.1063/1.3183938

View online: http://dx.doi.org/10.1063/1.3183938

View Table of Contents: http://scitation.aip.org/content/aip/journal/jap/106/3?ver=pdfcov

Published by the AIP Publishing

Multiple scattering x-ray photoelectron diffraction study of the $SrTiO_3(100)$ surface

A. Pancotti,[1] N. Barrett,[2,a)] L. F. Zagonel,[2] and G. M. Vanacore[3]
[1]*Instituto de Fisica, Universidade Estadual de Campinas, C.P. 6165, Campinas-Unicamp, Sao Paulo 13083-970, Brazil*
[2]*CEA DSM/IRAMIS/SPCSI, CEA Saclay, 91191 Gif sur Yvette, France*
[3]*Dipartimento di Fisica, Politecnico di Milano, Piazza Leonardo da Vinci, 32, 20133 Milano, Italy*

(Received 17 April 2009; accepted 23 June 2009; published online 4 August 2009; publisher error corrected 5 August 2009)

The atomic surface structure of $SrTiO_3(100)$ after annealing at 630 °C in vacuum is investigated by x-ray photoelectron diffraction (XPD) using the Sr $3d_{5/2}$ core level. The photoelectron diffraction peaks are successfully assigned by considering the forward scattering of photoelectrons by the atomic potential near the emitter atom in the lattice. The strongest diffraction peaks are aligned along the single crystal internuclear axes. We compare the results of photoelectron multiple scattering calculations (MSC) of SrO and TiO_2 terminated $SrTiO_3(100)$ surfaces, including surface relaxation and rumpling, with the experimental data. For TiO_2 and SrO terminated $SrTiO_3(100)$ surfaces, all top-layer cations relax inward, whereas second-layer atoms relax outward. The surface rumpling for SrO- and TiO_2-terminated surfaces agrees well with low-energy electron diffraction results. Using a genetic algorithm the best agreement of MSC to the experimental XPD data is obtained for a SrO terminated surface with a 30% coverage of 3 ML SrO(100) islands. © *2009 American Institute of Physics*. [DOI: 10.1063/1.3183938]

I. INTRODUCTION

$SrTiO_3$ has attracted considerable interest in the microelectronics industry because of the need for materials which have small leak currents. Furthermore, it is used on a large scale as substrate material for the growth of thin film perovskitelike materials, such as high-T_c superconductors. In both cases the control of the surface structure is of great interest.[1]

Strontium titanate, $SrTiO_3$ (STO), is a model for perovskite-type oxides of general formula ABO_3. The A and B cation sites are occupied by elements with different valences and different ionic radii which determine to a large extent the properties and structures of these materials. The atomic structure of STO, given in Fig. 1(a), can be seen as a network of sixfold oxygen coordinated titanium atoms, with strontium in the interstitial sites, leading to alternating TiO_2 and SrO layers in a ⟨100⟩ direction. Bulk STO has a $Pm3m$ space group, with lattice parameter $a=3.901$ Å at room temperature.

Thus, the ideal STO (100) surface termination layer can be either TiO_2 or SrO. Different preparation methods and analysis techniques have been employed to elucidate the nature of the (100) surface and well ordered surfaces can now be obtained.[2] However, the detailed surface atomic structure is still a matter of debate. For example, reconstruction occurs depending on the annealing conditions.[3] Most studies agree on the important role of oxygen vacancies in the mechanism of reconstruction, while Kubo and Nozoye[4] proposed a model in which an ordered Sr adatom structure occurs on the surface.

Experimentally, a single surface termination can be obtained by a combination of chemical etching and annealing. Recently, various studies[5–8] have also reported that after heat treatment, new phases appear on the STO(100) surface. Szot *et al.*[5] found that in an oxidizing atmosphere, SrO_x segregates on the surface in liquid form but during prolonged annealing the droplets crystallize, as SrO. They also observed[5,7,8] that when annealed between 800 and 1000 °C under oxidizing conditions, the surface is SrO-rich exhibiting Ruddlesden–Popper (RP) phases,[9] i.e., surface layers with the stoichiometry $Sr_{n+1}Ti_nO_{3n+1}$ formed by inserting extra SrO layers in the $SrTiO_3$ sequence of layers in the [001] direction, whereas under reducing conditions, Ti-rich phases (TiO and TiO_2) can form on and near the surface. Gunhold *et al.*[6] also reported the formation of SrO_x islands on the annealed (100) surface and annealing in ultrahigh vacuum (UHV) led to Ti_2O_3 and SrO island formation on the surface. However, there seems to be now general consensus[10–15] that the surface layer of annealed $SrTiO_3(100)$ is Sr rich. Two experimental studies,[10,16] for example, reported surface layers of the (100) crystal similar to RP phases. In a recent

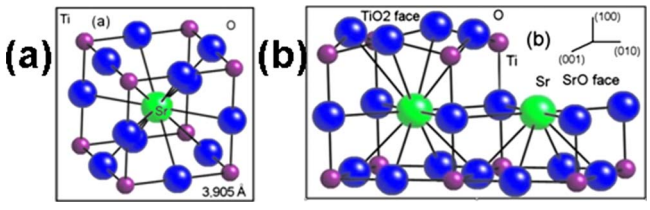

FIG. 1. (Color online) (a) Unit cell for STO cubic lattice. (b) Schematic of possible STO(100) surface termination. Rumpled structure is emphasized only for the TiO_2 face.

a)Author to whom correspondence should be addressed. Electronic mail: nick.barrett@cea.fr.

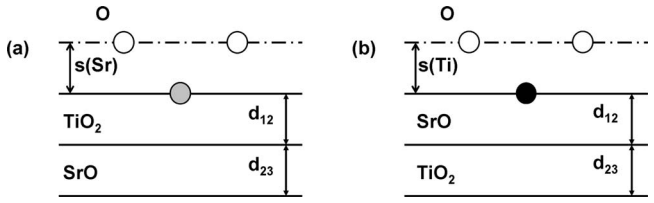

FIG. 2. Schematic of (a) the SrO-terminated and (b) TiO_2-terminated STO(100) surfaces showing the structural parameters describing the near-surface interplanar relaxation (d_{12}, d_{23}, d_{34}, d_{45}, and d_{56}) and the surface rumpling [s(Sr) and s(Ti)].

investigation, two different terminations, SrO_x and TiO_2, have been identified on samples annealed in UHV at temperatures <500 °C.[17]

Previous work using a variety of techniques has calculated or measured with some success relaxations in the surface structure.[18–24] Ideal (100) surface terminations are nearly neutral, however, charge neutrality may be affected by two, related, phenomena. On the one hand, surface enhanced covalency may induce deviations from integer ionic charge,[25,26] on the other hand, systematic longitudinal relaxation of one ion species with respect to the other or "rumpling," as shown in Fig. 1(b), can create a surface dipole. Thus, although STO is paraelectric at room temperature, such a dipole may give rise to surface ferroelectricity, with potentially important consequences for epitaxial growth of magnetic or superconducting oxides. The amplitudes of surface rumpling s (the relative displacement of oxygen with respect to metal atom in the surface layer) and the changes in internal layer distances d_{ij} (i and j are the layer indices) are defined in Fig. 2. The known experimental results for surface rumpling s and the changes in internal layer distances d_{ij} are summarized in Table I. Titanium atoms in the bulk state have six nearest oxygen atoms forming an octahedral. However, at the surface, one nearest oxygen atom is missing, namely, the Ti–O bond is cut in the z direction. Therefore, the surface Ti atoms are likely to be contracted into the substrate for a better hybridization with the remaining oxygen neighbors. On the other hand, reflection high energy electron diffraction (RHEED) measurements concluded that the distances s, Δd_{12}, Δd_{23} are expanded.[22] However, the high kinetic energy of electrons in the RHEED may make them less sensitive to the more external layers.[22] An extremely detailed surface x-ray diffraction study of hot STO(001) using a different initial surface preparation has shown a double TiO_2 terminating layer with opposite surface rumpling to that described above.[27]

In order to provide further experimental data on surface rumpling and relaxation, we use x-ray photoelectron diffraction (XPD) on the Sr $3d_{5/2}$ core level to study the details of the STO(100) surface after annealing in UHV. In XPD, the angular dependence of the collected electron intensity originates from the interference of the directly emitted photoelectron wave and the scattered electron waves. XPD is sensitive on an atomic scale; it can be used to analyze local atomic structure down to the monolayer and surface relaxation. Quantitative information may be obtained using electron scattering simulations, however, when compared to experimental results, the "forward focusing" intensity is overemphasized in single scattering calculations. Scattering at the first few atoms along a row of atoms focuses the emission in the emitter-scatterer direction, but subsequent atoms tend to defocus the signal. The defocusing is linked to the development of the conventional Kikuchi bands which become more intense when the forward-scattering peak intensity diminishes. The large number of elastic scattering events make it is necessary to use multiple scattering calculations (MSCs).[28] In all calculations, we used six multiple scattering events and expansions up to the fourth order Rehr–Albers.[28] In this paper we include surface relaxation of TiO_2-terminated and SrO-terminated STO(100) surface in the simulation of the Sr $3d$ XPD experimental results. To our knowledge there is no previous XPD study of STO(100) in the literature.

After describing the experimental conditions used for the XPD data acquisition, the formalism used for the multiple scattering calculations is presented. In Sec. IV the results of

TABLE I. Surface rumpling s and displacement d_{ij} (as a percentage of bulk lattice constant) obtained from a genetic algorithm optimization of the XPD simulation for the three near-surface planes of SrO and TiO_2 terminated STO(100).

	SrO terminated			TiO_2 terminated		
	s	Δd_{12}	Δd_{23}	s	Δd_{12}	Δd_{23}
This work	4.3 ± 1.0	-1.6 ± 1.3	1.0 ± 1.0	2.9 ± 1.0	-5.7 ± 1.0	6.3 ± 1.1
Ab initio[a]	5.7	−6.7	2.6	1.9	−7.1	3.1
Ab initio[b]	7.7	−2.8	1.3	2.0	−1.10	2.8
Shell model[c]	8.2	−8.6	3.0	1.2	−6.4	4.0
LEED[d]	4.1 ± 2	-5.0 ± 1.0	2.0 ± 1.0	2.1 ± 1.0	1.0 ± 1.0	-1.0 ± 1.0
RHEED[e]	4.1 ± 0.6	2.6 ± 0.6	1.3 ± 1.3	2.6 ± 0.6	1.8 ± 0.6	1.3 ± 1.3
MEIS[f]	⋯	⋯	⋯	3.1 ± 0.4	2.7 ± 0.2	⋯
SXRD[g]	1.3 ± 12.1	-4.1 ± 3.6	$+2.1 \pm 2.8$	12.8 ± 8.5	4.86 ± 1	⋯

[a]Reference 18.
[b]Reference 19.
[c]Reference 20.
[d]Reference 21.
[e]Reference 22.
[f]Reference 23.
[g]Reference 24.

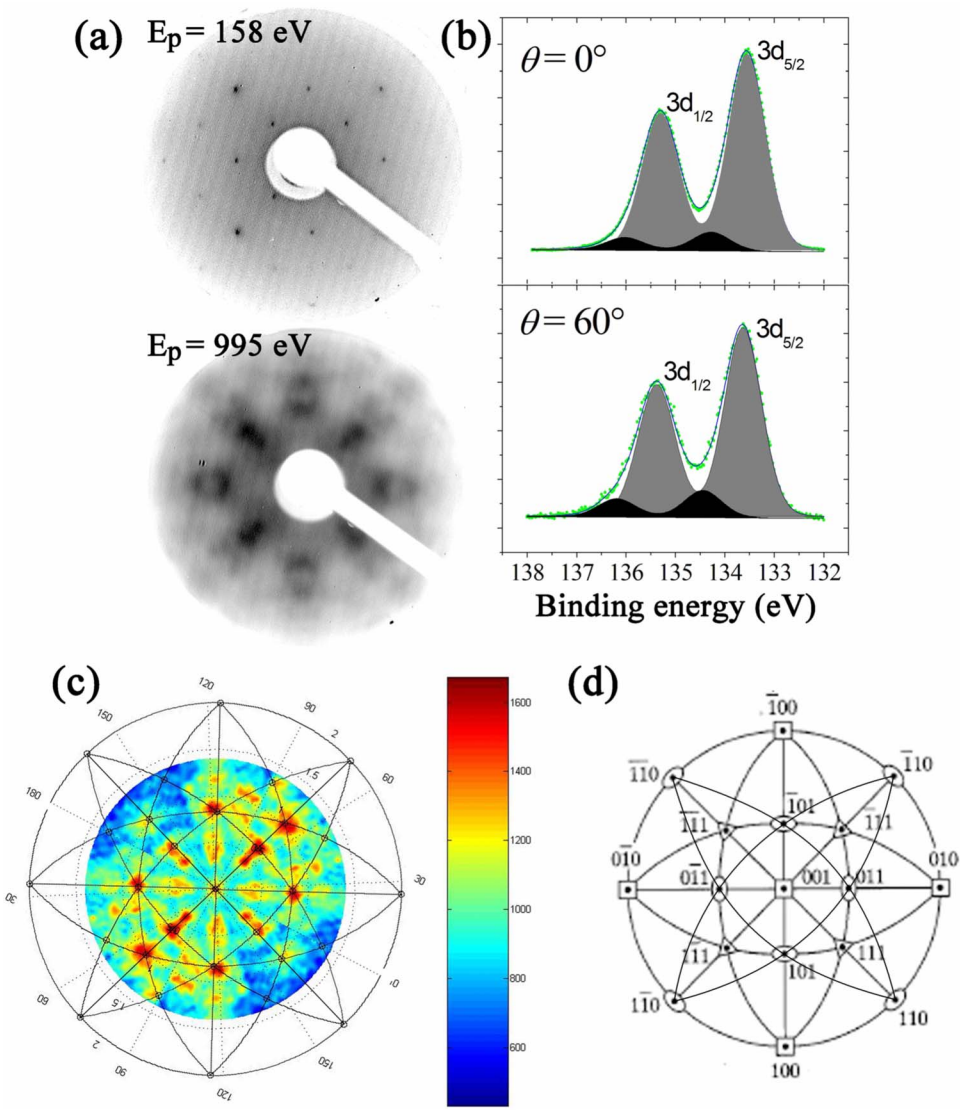

FIG. 3. (Color online) (a) (1×1) LEED pattern from the STO (100) surface for primary electron energies of 158 and 995 eV after annealing at 630 °C in UHV; (b) Sr 3*d* XPS spectrum at normal and 60° (surface sensitive) detection angles showing the presence of a Sr surface component (black shading); (c) experimental Sr $3d_{5/2}$ photoelectron intensity map; (d) location of high-density crystal axes and planes in the projection of (c).

multiple scattering calculations for diffraction (MSCD) simulations are presented and refined, to obtain a detailed interpretation of the experimental results.

II. EXPERIMENTAL

Pure STO has a 3.2 eV band gap which makes it unsuitable for x-ray photoelectron spectroscopy (XPS)/XPD experiments due to sample charging. To overcome this problem the STO was doped with 0.5 wt % Nb. The sample was furnished by SurfaceNet GmbH. The Nb doped STO single crystal was mounted and aligned *in situ* with a diode laser so as the surface normal was within 1° of the axial axis of rotation.

The XPD chamber was equipped with a sample heating facility up to about 1200 K and ion gun for sample cleaning. The sample was cleaned by *in situ* annealing at 630 °C for $1\frac{1}{2}$ h until all traces of impurities as seen by XPS were removed. The low enery electron diffraction (LEED) pattern for 158 eV primary electron energy [Fig. 3(a)] for STO(100) has a perfect (1×1) symmetry reflecting a well ordered surface after annealing, consistent with a SrO surface termination. The sample crystallinity is confirmed by the high energy (995 eV) LEED pattern shown in Fig. 3(a), which also has similar depth sensitivity to the Al $K\alpha$ excited XPD signal. No shift was observed in the Nb^{5+} 3*p* XPS spectrum, excluding Nb segregation during annealing.[29] A high resolution Sr 3*d* photoemission spectrum clearly shows the presence of a surface related component, see Fig. 3(b). The spin orbit splitting is 1.8 eV and the measured surface core level shift is about 0.8 eV. At 60° off normal detection, the high binding energy component increases in intensity, confirming that it is due to surface atoms.

The XPD analysis was done at a base pressure of 5×10^{-8} Pa, the analyzer acceptance angle was ±1.0°, and was used in the fixed transmission mode with pass energy of 40 eV.

The sample is mounted on a high precision manipulator with full polar and azimuthal rotations. To determine the surface structure, the XPD anisotropy of the Sr 3*d* emission was

measured over a wide range of polar and azimuthal angles with an angular resolution of $\pm 1°$. For each (θ, ϕ) point both the core level and the background intensities are recorded. The intensities of the photoelectron peak versus direction are plotted and show strong diffraction effects. The crystal is rotated around the surface normal, changing the azimuthal angle ϕ for a given polar angle θ, the polar angle is then incremented, and the azimuthal scan repeated with the appropriate ϕ step. Thus the two-dimensional diffraction maps are measured by concatenating the different azimuthal scans: The initial polar angle is $\theta_{max}=68°$. As θ is reduced toward normal emission, the ϕ step is adjusted in order to give uniform solid angle sampling above the sample surface.[30] The raw data are shown in Fig. 3(c) where the angular coordinates are projected using the following transformations: $x=2\tan(\theta/2)\cos\varphi$ and $y=2\tan(\theta/2)\sin\varphi$. The positions of the high-density crystal planes and axes are indicated in Fig. 3(d). The ⟨100⟩-, ⟨110⟩-, and ⟨111⟩-like directions are visible in the experimental data, as are structures corresponding to the {111} set of planes. The full (ϕ, θ) space is explored.

III. MULTIPLE SCATTERING SIMULATIONS

XPD simulations of the STO(100) surface are complex due to the large parameter space. The surface termination, SrO or TiO_2, or a combination of both must be tested. The two basic surface terminations are shown in Fig. 2. The possibility of SrO(100) surface segregation must be tested in each case. Finally, interplanar relaxation in the surface region and surface rumpling should be taken into account. This results in an extremely large parameter space and extortionate calculation times. We have adopted a simulation strategy which allows testing in parallel of, on the one hand, the surface rumpling and relaxation, and, on the other, the surface termination. The best simulation is then obtained by combining the two final solutions in a last iteration.

The XPD simulations were done using the cluster model approach of the MSCD code[28] based on the muffin-tin potential approximation. Two paraboloidal clusters were used. The first one had a surface radius of 22 Å and a depth of 10 Å and contained 900 atoms. It was used to investigate changes in the interplanar distances and surface rumpling, starting from the unrelaxed surface of the bulk structure.[31] The second one was used for the final simulation of the experimental result, including not only the surface relaxation but also bulk photoelectron diffraction. This cluster has 402 atoms, a depth of 22 Å, and radius 10 Å, sufficiently large to ensure convergence of the scattering calculation and to avoid cluster border effects. In Fig. 4 we show the second cluster with, in this case, a SrO terminated STO(100) surface. There are thus five emitting layers in the final cluster, which proved sufficient to simulate the XPD pattern. Additional emitters did not improve significantly the results. We note that the electron kinetic energy for Sr $3d_{5/2}$ excited with Al $K\alpha$ radiation gives a photoelectron inelastic mean free path of about 20 Å.

The band gap, lattice parameter, and inner potential were set to the tabulated bulk values. The calculations were performed for a temperature $T=300$ K. The surface potential V_0, which accounts for refraction at the surface/vacuum step,

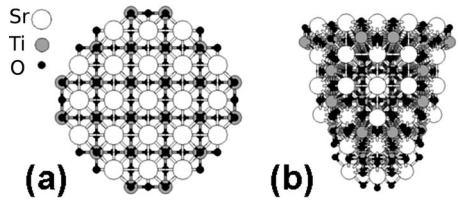

FIG. 4. 402 atom cluster of the STO(100) surface with surface termination SrO used for simulation of the XPD anisotropy: (a) top view and (b) lateral view. Black color corresponds to oxygen atoms, white to strontium atoms, and gray to titanium atoms.

and the Debye temperatures (θ_D) were adjustable parameters. The values obtained were $V_0=10.5$ eV and $\theta_D=147$, 420, and 80 K for Sr, Ti, and O atoms, respectively, in good agreement with literature.[32]

In order to account for surface relaxation, we allowed atoms of two outermost surface layers to relax along the z axis. We then extended relaxation to the third to fifth subsurface layers. Atoms are fixed at their lateral bulk positions and allowed to relax in the z direction. The structure is determined in a fit procedure that searches for the set of parameters that optimizes the agreement between the theoretical and experimental diffraction curves, through minimization of the reliability factor R_a, defined as the difference between the experimental and the simulated diffraction patterns,[28]

$$R_a = \sum_i \frac{[\chi_c^i(\theta,\phi) - \chi_e^i(\theta,\phi)]^2}{\chi_c^i(\theta,\phi)^2 + \chi_e^i(\theta,\phi)^2}.$$

The quantities χ_c^i and χ_e^i are, respectively, the calculated and experimental photoelectron diffraction anisotropies (see below). The smaller the R_a factor, the better the agreement with experiment, with $0 \le R_a \le 1$. A perfect agreement corresponds to $R_a=0$, no agreement is expressed by $R_a=1$. The sum in the R_a equation is over all angles in the database.

As a further measure of the quality of the analysis beyond the numerical value of the R-factor, uncertainties can be estimated using the steepness of the R-factor space assigned to a parameter in the vicinity of its absolute minimum and the maximum number of separable diffraction information N with an experimental data set,

$$\mathrm{Var}(R_{\min}) = R_{\min}\sqrt{2/N},$$

where $\mathrm{Var}(R_{\min})$ denotes the variance of R at its minimum. This procedure was introduced by Pendry[33] for quantitative LEED analysis and was adapted to XPD.[34] A study of the uncertainties in this context has been done by Van Hove *et al.*[35]

To find the best parameters in our relaxations in the simulations with MSCD code, we used a genetic algorithm.[36] Genetic algorithms are very useful when applied to optimization problems that require an extensive search in a parameter space that presents several local minima. The genetic algorithm was used to optimize the relaxation of the interlayer distances of the model clusters with five different variables (d_{12}, d_{23}, d_{34}, d_{45}, and d_{56}), thus minimizing R_a-factor analysis.

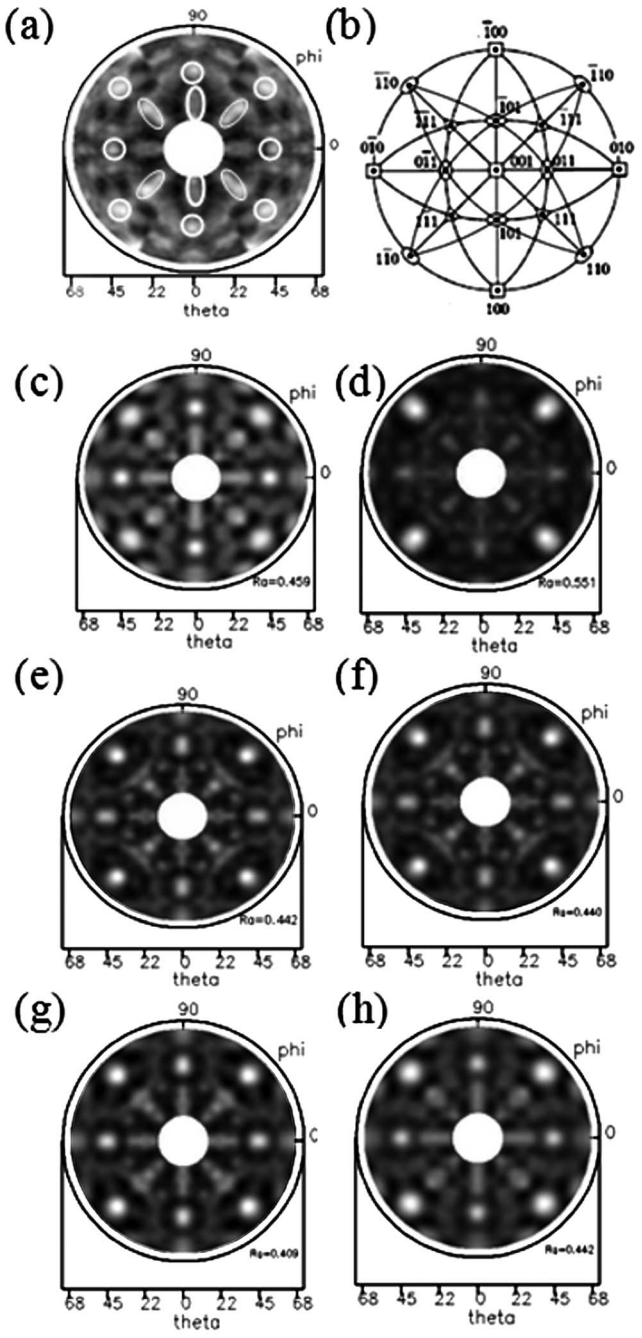

FIG. 5. (a) Experimental XPD anisotropy for Sr $3d_{5/2}$ excited with Al $K\alpha$ radiation together with the principal crystal directions and (b) location of high-density crystal planes. MSCD theory for (c) STO(100) with surface termination SrO, (d) STO(100) with surface termination TiO_2, (e) SrO(100) structure (lattice parameter of 5.1040 Å). The last three patterns are linear combinations of (f) TiO_2 and SrO terminations, (g) SrO(100) islands and SrO termination, and (h) SrO(100) islands and TiO_2 termination.

IV. RESULTS AND DISCUSSION

In the Fig. 5(a) we present the experimental Sr $3d_{5/2}$ photoelectron diffraction patterns over the polar angle range $16° \leq \theta \leq 68°$. The center of each plot represents normal emission; the edge represents grazing angle emission. For the purposes of comparison with the simulations, the data have been symmetrized by a mirror reflection. Since STO(100) contains such a mirror plane, this operation is not expected to result in lost structure. The kinetic energy of photoelectrons is 1353.6 eV. The background subtracted Sr $3d_{5/2}$ intensity is represented by a linear gray scale.

In order to compare the simulations directly with the experimental data, the XPD intensities are presented in the form of an anisotropy. The anisotropy χ is defined as

$$\chi(\theta,\varphi,\vec{k}) = \frac{I(\theta,\varphi,\vec{k}) - I_o(\theta,\varphi,\vec{k})}{I_o(\theta,\varphi,\vec{k})},$$

where $I(\theta,\varphi,\vec{k})$ is the measured or calculated photoemission intensity and $I_o(\theta,\varphi,\vec{k})$ is the photoelectron intensity in the absence of diffraction (free atom). In our case we have taken the azimuthal average of intensities at each polar angle, fitted the entire average data set with a low order spline function in θ and treated the result as the intensity in the absence of diffraction. For convenience, the crystal directions are reproduced in Fig. 5(b).

The initial structure for the relaxation simulation was an ideal STO surface with atomic positions corresponding to those of bulk STO(100). Using the shallow, surface-sensitive paraboloid, at the surface layer, all atoms are pushed into the substrate compared with ideal surface, the titanium and strontium atoms move deeper than oxygen atoms, leading to a surface rumpling $s(\text{Ti})=0.110$ Å and $s(\text{Sr})=0.168$ Å, respectively, for TiO_2 and SrO terminations. The interlayer distances d_{12} is reduced while d_{23} expanded. We have also allowed relaxation of deeper subsurface distances d_{34}, d_{45}, and d_{56}. Further relaxation does not improve the simulation, in agreement with the number of relaxed layers found by Heifets *et al.*[20]

It is important to emphasize that the surface relaxation obtained using the genetic algorithm significantly improves the agreement between simulation and experiment. For example, the unrelaxed SrO terminated surface with a 30% SrO island coverage gives a mean R_a averaged over all polar angles of 0.48. After relaxation the mean R_a factor decreases to 0.38. Not surprisingly, the R_a factor increases in all cases with polar angle, for the unrelaxed surface it varies from 0.20 near normal emission to 0.80 at high polar angles, whereas after relaxation it varies between 0.17 and 0.53, supporting the presence of significant surface relaxation.

Table I shows that the MSCD simulations agree well with previous results in the literature. We obtain the same sign and magnitudes for both the rumpling s and change in interlayer distances Δd. The interlayer distances d_{12} is reduced by 1.6% of the bulk lattice parameter to 1.89 Å while d_{23} appears expanded by 1.0% of the bulk lattice parameter to 1.99 Å. The amplitude of surface rumpling s (the relative displacement of oxygen with respect to metal atom in the surface layer) is calculated to be 4.3%. For the SrO terminated surface, the values are smaller than those obtained from *ab initio* and shell model calculations, but significantly closer to results deduced from quantitative LEED analysis, with the added advantage of a considerably smaller uncertainty. In the case of a TiO_2 surface termination, the XPD simulation suggests a larger interplanar relaxation than that calculated by theory and observed experimentally. The deduced interplanar distances and their uncertainties are given in Table II.

TABLE II. Calculated structure parameters for the relaxed TiO_2 and SrO terminated STO surfaces.

	Interplanar distance (Å)				
	d_{12}	d_{23}	d_{34}	d_{45}	d_{56}
SrO-terminated	1.89 ± 0.05	1.99 ± 0.04	1.92 ± 0.04	1.99 ± 0.05	1.91 ± 0.05
TiO_2-terminated	1.73 ± 0.04	2.20 ± 0.04	1.98 ± 0.05	1.59 ± 0.05	2.26 ± 0.05

The statistical errors associated with parameters were estimated by considering all values giving structures with R factors within the sum of the R factor minimum $R_{\min}$ and its variance $\mathrm{Var}(R_{\min})$, as falling within one standard deviation of the corresponding parameter value of the best-fit geometry. The same statistical uncertainties are obtained using the MSCD program for both SrO and TiO_2 surface terminations.

To determine the final structure we then included the relaxation and rumpling results into the surface termination models using the deeper paraboloidal cluster.

The MSCD simulations are shown in Figs. 5(c)–5(h). Figure 5(c) shows the best simulation for a perfectly SrO terminated surface of STO. Figure 5(d) is the corresponding result for a TiO_2 terminated surface of STO. SrO(100) island formation on the SrO terminated surface of STO(100) is shown in Fig. 5(e).

The best result for a linear combination of the two basic surface terminations, SrO (95%) and TiO_2 (5%), is shown in Fig. 5(f). The agreement between simulation and experiment is further improved by including SrO(100) islands covering 30% of the pure SrO termination [Fig. 5(g)]. An SrO(100) island coverage of 75% on the pure TiO_2 termination also gives a good agreement [Fig. 5(h)], however, the high resolution XPS spectra clearly suggest the presence of a Sr surface component and show no evidence for a significant surface component in the Ti $2p$ spectra (not shown). Furthermore the LEED pattern in Fig. 3 supports the interpretation of a SrO surface termination.

The variation of the R_a factor as a function of the SrO(100) island coverage and geometry is shown in Fig. 6. The upper inset shows that in the presence of SrO islands, a minimum R_a factor is found for 3 ML high islands. The lower inset shows that an island radius of 10 Å minimizes the R_a factor. The main figure shows the R_a factor as a function of the fractional 3 ML high, 20 Å diameter SrO(100) island coverage on SrO and TiO_2 terminated surfaces. For comparison, the R_a factor for linear combinations of SrO and TiO_2, without islands, is also included.

In order to illustrate further the agreement, we display in Fig. 7 a comparison between simulation including relaxation for the range of model surfaces used and experiment at four different polar angles: (a) 26°, (b) 34°, (c) 44°, and (d) 54°. In each panel the experimental anisotropy is compared with the simulations (solid lines) for (from top to bottom): TiO_2 termination plane, SrO termination plane, SrO(100) island termination, linear combinations of SrO (95%) and TiO_2 (5%), TiO_2 terminated STO (25%) with SrO(100) (75%), and finally SrO terminated STO (70%) with SrO(100). The last two simulations represent the situation of a single surface termination with SrO(100) islands. We note that it would be insufficient to base the refinement on a narrow range of polar angles. At 26°, the best R_a factor is obtained for the pure SrO termination or for a linear combination of SrO and TiO_2 heavily weighted in favor of SrO. On the other hand, at 34°, it is the TiO_2 termination with SrO(100) islands which gives one of the best R_a factors. A realistic solution can be obtained only by looking at the R_a factor over a wide range of polar angles. The higher polar angle region seems particularly sensitive to the rumpling and to the SrO(100) island segregation.

Thus, after annealing at 630 °C in UHV, the best agreement between simulation and experiment is given by a SrO surface termination, with the segregation of 3 ML SrO(100) islands covering about 30% of the surface. This solution is shown schematically in Fig. 8, although the R_a factor analysis does suggest that a small proportion of the surface may be TiO_2 terminated. The interlayer distances d_{12} is reduced by 3.3% with respect to the unrelaxed, bulk value to 1.89 Å, while d_{23} appears expanded by 2.2% to 1.99 Å. The amplitude of surface rumpling s (the relative displacement of oxygen with respect to metal atom in the surface layer) is calculated to be 4.3%.

Our results agree well with the *ab initio* calculations of Padilla *et al.*[18] and Cheng *et al.*[19] Using the notion of effective charge, the latter has calculated the increase in the surface dipole due to rumpling to be 0.11 Å per surface unit cell, with contributions coming from as deep as four atomic layers. Although this is an order of magnitude less than the

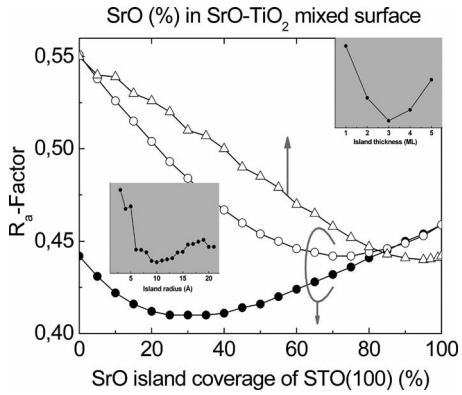

FIG. 6. R_a-factor analysis of the Sr $3d$ emission with $h\nu = 1486.6$ eV for a surface coverage of 3 ML SrO(100) islands on a pure SrO termination (full circles) indicating a minimum for a SrO(100) island coverage of 30%; surface coverage of 3 ML SrO(100) islands on a pure TiO_2 termination (open circles), indicating a minimum for an island coverage of 75%; and a linear combination of a SrO(100) and TiO_2 termination (open triangles), indicating a shallow minimum for the SrO termination coverage of 95%. The insets show the preliminary R_a-factor analysis for SrO(100) islands on STO(100) as a function of the island height and of the island radius.

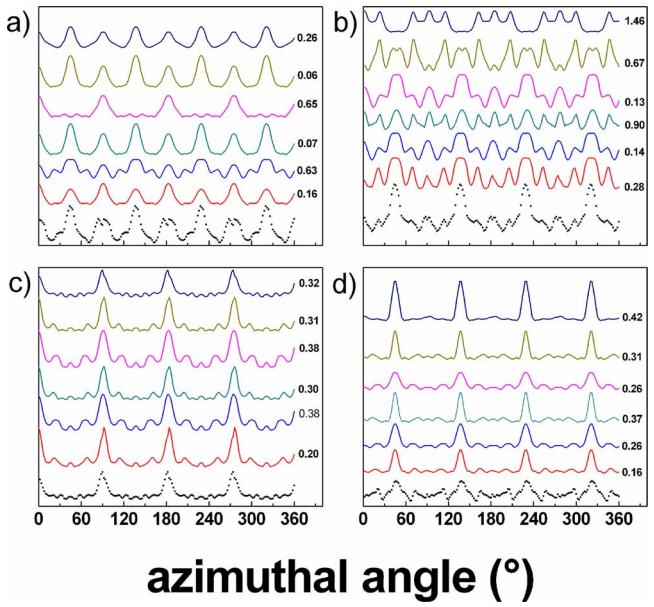

FIG. 7. (Color online) Comparison between simulation including relaxation for the range of model surfaces used and experiment (full circles) at four different polar angles: (a) 26°; (b) 34°; (c) 44°; and (d) 54°. In each figure the experimental anisotropy is compared with the simulations (solid lines) for (from top to bottom): TiO_2 termination plane, SrO termination plane, SrO(100) island termination, linear combinations of SrO (95%) and TiO_2 (5%), TiO_2 terminated STO (25%) with SrO(100) (75%), and finally SrO terminated STO (70%) with SrO(100). The last two simulations represent the situation of a single surface termination with SrO(100) islands.

dipole expected in ferroelectric $BaTiO_3$, it is far from being negligible. The surface rumpling as determined by XPD suggests similar values of dipole enhancement, thus the view of the STO(100) surface being neutral should be revised. Furthermore, it would be interesting to study the role of such surface ferroelectricity in distortions of the crystal field in, for example, epitaxial magnetic thin film oxides on STO substrates.

V. CONCLUSIONS

LEED and XPD show that annealing at 630 °C under vacuum leads to the (1×1) reconstruction of a flat, clean, and ordered SrO terminated STO(100) surface. LEED patterns and surface shifts in Sr $3d_{5/2}$ XPS are consistent with SrO termination. The XPD patterns of Sr $3d_{5/2}$ photoelectron signal were used in order to investigate the details of the surface structure. The kinetic energy of the photoelectron ($\sim$1 keV) enhances forward scattering, giving strong diffraction peaks along the directions of low Miller index internuclear axes. For a quantitative analysis, the experimental diffraction pattern was compared to simulated patterns for structural models within a comprehensive R_a-factor analysis. Linear combinations of SrO and TiO_2 surface terminations with SrO(100) islands are used to find the best agreement with experiment. A genetic algorithm was used to probe the large parameter space of interlayer distances. The interlayer distance d_{12} is reduced by 1.6% of the bulk lattice parameter to 1.89 Å, while d_{23} appears expanded by 1.0% to 1.99 Å. The amplitude of surface rumpling s (the relative displacement of oxygen with respect to metal atom in the surface layer) is calculated to be 4.3%. The best simulation is obtained for a SrO terminated surface with a 30% coverage of 3 ML high SrO(100) islands, including interlayer relaxation and rumpling. The detailed information on the surface termination may be important for the interface chemistry on epitaxial growth of magnetic, superconducting, or ferroelectric thin films on STO.

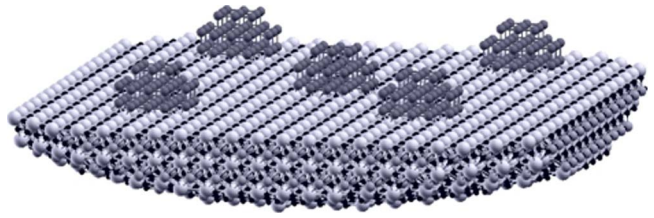

FIG. 8. (Color online) Schematic of the best MSCD simulation of the surface structure. The surface is SrO terminated with approximately 30% SrO(100) island coverage, of height of 3 ML.

ACKNOWLEDGMENTS

The authors would like to thank J. Leroy and B. Delomez for technical assistance. This work was financially supported by FAPESP under the doctorate Fellowship No. 0554993-4 and by the European Commission under contract No. NMP3-CT-2005-013862 (INCEMS).

[1] G. Rijnders, S. Curras, M. Huijben, D. Blanck, and H. Rogalla, Appl. Phys. Lett. **84**, 1150 (2004); D. E. Kotecki, J. D. Baniecki, H. Shen, R. B. Laibowitz, K. L. Saenger, J. J. Lian., T. M. Shaw, S. D. Athavale, C. Cabral Jr., P. R. Duncombe, M. Gutsche, G. Kunkel, Y.-J. Park, Y. Y. Yang, and R. Wise, IBM J. Res. Dev. **43**, 367 (1999).
[2] M. Kawasaki, A. Ohtomo, T. Arkane, K. Takahashi, M. Yoshimoto, and H. Koinuma, Appl. Surf. Sci. **107**, 102 (1996).
[3] N. Erdman and L. D. Marks, Surf. Sci. **526**, 107 (2003).
[4] T. Kubo and H. Nozoye, Phys. Rev. Lett. **86**, 1801 (2001).
[5] K. Szot, W. Speier, U. Breuer, R. Meyer, J. Szade, and R. Waser, Surf. Sci. **460**, 112 (2000).
[6] A. Gunhold, K. Gomann, L. Beuermann, M. Frerichs, G. Borchardt, V. Kempter, and W. Maus-Friedrichs, Surf. Sci. **507–510**, 447 (2002).
[7] K. Szot and W. Speier, Phys. Rev. B **60**, 5909 (1999).
[8] M. R. Castell, Surf. Sci. **516**, 33 (2002).
[9] S. N. Ruddlesden and P. Popper, Acta Crystallogr. **11**, 54 (1958).
[10] Y. Liang and D. Bonnell, Surf. Sci. **285**, L510 (1993).
[11] V. E. Henrich, G. Dresselhaus, and H. J. Zeiger, Phys. Rev. B **17**, 4908 (1978).
[12] T. Matsumoto, H. Tanaka, T. Kawai, and S. Kawai, Surf. Sci. **278**, L153 (1992).
[13] Y. Haruyama, H. Fukutani, Y. Aiura, Y. Nishihara, T. Komeda, S. Kodaira, T. Maryama, and H. Kato, Jpn. J. Appl. Phys., Suppl. **32**, L543 (1993).
[14] A. Hirata, K. Saika, A. Koma, and A. Ando, Surf. Sci. **319**, 267 (1994).
[15] L. F. Zagonel, N. Barrett, O. Renault, A. Bailly, M. Bäurer, M. Hoffmann, S.-J. Shih, and D. Cockayne, Surf. Interface Anal. **40**, 1709 (2008).
[16] K. Szot, W. Speier, J. Herion, and C. Freiburg, Appl. Phys. A: Mater. Sci. Process. **64**, 64 (1997).
[17] J. Fompeyrine, R. Berger, H. P. Lang, J. Perret, E. Machler, Ch. Gerber, and J.-P. Locquet, Appl. Phys. Lett. **72**, 1697 (1998).
[18] J. Padilla and D. Vanderbilt, Surf. Sci. **418**, 64 (1998).
[19] C. Cheng, K. Kunc, and M. H. Lee, Phys. Rev. B **62**, 10409 (2000).
[20] E. Heifets, E. A. Kotomin, and J. Maier, Surf. Sci. **462**, 19 (2000).
[21] N. Bickel, G. Schmidt, K. Heinz, and K. Muller, Phys. Rev. Lett. **62**, 2009 (1989).
[22] T. Hikita, T. Hanada, M. Kudo, and M. Kawai, Surf. Sci. **287–288**, 377 (1993).
[23] A. Ikeda, T. Morishita, and Y. Kido, Surf. Sci. **433–435**, 520 (1999).
[24] G. Charlton, S. Brennan, C. A. Muryn, R. McGrath, D. Norman, T. S. Turner, and G. Thornton, Surf. Sci. **457**, L376 (2000).
[25] F. Bottin, F. Finocchi, and C. Noguera, Phys. Rev. B **68**, 035418 (2003).

[26]R. I. Eglitis and D. Vanderbilt, Phys. Rev. B **77**, 195408 (2008).
[27]R. Herger, P. R. Willmott, O. Bunk, C. M. Schlepütz, B. D. Patterson, B. Delley, V. L. Shneerson, P. F. Lyman, and D. K. Saldin, Phys. Rev. B **76**, 195435 (2007).
[28]Y. Chen and M. V. Hove, MSCD Package, Lawrence Berkeley National Laboratory, 1998, http://www.ap.cityu.edu.hk/personal-website/Van-Hove_files/mscd/mscdpack.html.
[29]P. Pasierb, S. Komornicki, and M. Rekas, J. Phys. Chem. Solids **60**, 1835 (1999).
[30]A. De Siervo, E. Soares, R. Landers, and G. G. Kleiman, Phys. Rev. B **71**, 115417 (2005).
[31]R. H. Mitchell, A. R. Chakhmouradian, and P. M. Woodward, Phys. Chem. Miner. **27**, 583 (2000).
[32]From the Integral Scientist Periodic Table of the Elements (ISPT), available on http://www.qivx.com.
[33]J. Pendry, J. Phys C **13**, 937 (1980).
[34]F. Bondino, G. Comelli, A. Baraldi, R. Rosei, S. Lizzit, A. Goldoni, R. Larciprete, and G. Paolucci, Phys. Rev. B **66**, 075402 (2002).
[35]M. Van Hove, W. Moritz, H. Over, P. Rous, A. Wander, A. Barbieri, N. Materer, U. Starke, and G. Somorjai, Surf. Sci. Rep. **19**, 191 (1993).
[36]M. L. Viana, R. Diez Muino, E. A. Soares, M. A. Van Hove, V. E. de Carvalho, J. Phys.: Condens. Matter **19**, 446002 (2007).